

# The Effect of Determining Topography Parameters on Analyzing Elastic Contact Between Isotropic Rough Surfaces

**Gorakh Pawar**

Department of Mechanical Engineering,  
University of Utah,  
Salt Lake City, UT 84112

**Pawel Pawlus**

Rzeszow University of Technology,  
Department of Manufacturing  
Processes and Production Organisation,  
Rzeszow, Poland

**Izhak Etsion**

Department of Mechanical Engineering,  
Technion – Israel Institute of Technology,  
Haifa, Israel

**Bart Raeymaekers**

Department of Mechanical Engineering,  
University of Utah,  
Salt Lake City, UT 84112  
e-mail: bart.raeymaekers@utah.edu

*The elastic contact between two computer generated isotropic rough surfaces is studied. First the surface topography parameters including the asperity density, mean summit radius, and standard deviation of asperity heights of the equivalent rough surface are determined using an 8-nearest neighbor summit identification scheme. Second, many cross sections of the equivalent rough surface are traced and their individual topography parameters are determined from their corresponding spectral moments. The topography parameters are also obtained from the average spectral moments of all cross sections. The asperity density is found to be the main difference between the summit identification scheme and the spectral moments method. The contact parameters such as the number of contacting asperities, real area of contact, and contact load for any given separation between the equivalent rough surface and a rigid flat are calculated by summing the contributions of all the contacting asperities using the summit identification model. These contact parameters are also obtained with the Greenwood-Williamson (GW) model using the topography parameters from each individual cross section and from the average spectral moments of all cross sections. Three different surfaces and three different sampling intervals were used to study how the method to determine topography parameters affects the resulting contact parameters. The contact parameters are found to vary significantly based on the method used to determine the topography parameters, and as a function of the autocorrelation length of the surface, as well as the sampling interval. Using a summit identification model or the GW model based on topography parameters obtained from a summit identification scheme is perhaps the most reliable approach.*

[DOI: 10.1115/1.4007760]

## 1 Introduction

Multiasperity elastic, elastic-plastic, and plastic contact models are used to predict contact parameters such as the real area of contact, normal load, and electrical conductivity as a function of the separation between contacting rough surfaces. Perhaps the most widely used multiasperity elastic contact model is the Greenwood-Williamson (GW) model [1]. The GW model considers an idealized isotropic three-dimensional (3D) rough surface with noninteracting (no bulk deformation) spherical asperity summits of constant radius, and with a Gaussian distribution of asperity heights. Since for isotropic rough surfaces the topography parameters are identical for all two-dimensional (2D) cross sections (traces) of this surface, the surface topography can be represented by any cross section of that surface. However, when characterizing an actual isotropic rough surface experimentally, or when analyzing a numerically generated isotropic rough surface, one finds that the topography parameters depend on the cross section from which they are derived. Hence, an ideal surface as the one used by GW may not exist. Although the original GW model has been successively improved by relaxing some of its simplifying assumptions [2–9], and entirely new theories have been developed [10,11], many researchers still apply the original GW model to simulate elastic contact of 3D isotropic rough surfaces [12–21].

The surface topography parameters of a rough surface are oftentimes calculated using the spectral moments approach described by McCool [12,14]. This method uses a single arbitrary 2D cross section of an isotropic rough surface to determine the asperity density  $\eta$ , mean summit radius  $\rho$ , and standard deviation of asperity heights  $\sigma_s$  of the entire 3D rough surface, see for instance [8,16,17,20,22,23]. Several authors have also used average values of the spectral moments obtained from a finite number of cross sections of the 3D surface to calculate the topography parameters; for example in [13,18,21,24,25]. Another method to determine the surface topography parameters is based on individually identifying the asperities [26–28]. The summits of the rough surface are identified as local maxima [26], and the topography parameters are calculated directly from these summits [8,27,28], as opposed to relying on statistical methods. Different  $N$ -nearest neighbor identification schemes can be used to identify local maxima, such as the 8-nearest neighbor [28–30] and the 4-nearest neighbor [28,29,31,32] schemes. The 8-nearest neighbor scheme seems to be the most accurate one [33].

Many authors continue to use the GW model to analyze the elastic contact of realistic 3D isotropic rough surfaces; hence implicitly assuming that the topography parameters of these rough surfaces are uniquely defined by a single arbitrary 2D cross section. However, as will be shown in this paper, significant differences may exist when calculating contact parameters using the GW model, depending on the method used to determine the surface topography parameters. No publications seem to exist in the open literature that evaluate the relative differences between the contact parameters obtained with the GW model for elastic contact of

Contributed by the Tribology Division of ASME for publication in the JOURNAL OF TRIBOLOGY. Manuscript received May 15, 2012; final manuscript received September 5, 2012; published online December 20, 2012. Assoc. Editor: Robert L. Jackson.

actual 3D isotropic rough surfaces, as a function of the method used to determine the topography parameters. This paper attempts to fill this gap and aims to provide an in-depth quantitative analysis of the different results obtained when calculating the relationship between the number of contacting asperities, the separation, the real area of contact, and the normal load, using different methods to determine the asperity density  $\eta$ , summit radius  $\rho$ , and standard deviation of asperity heights  $\sigma_s$  of the surfaces under analysis.

## 2 Methodology

Isotropic 3D rough surfaces with Gaussian distribution of asperity heights are numerically generated using the method described by Wu [34]. The topography parameters of the equivalent rough surface [3,14] of two contacting rough surfaces are then determined using the spectral moments method described by McCool [12,14] and a summit identification method [26–28]. Second, the equivalent rough surface is placed in contact with a rigid flat, and the relationship between the number of contacting asperities, real area of contact, normal load, and separation is computed with the GW model using the topography parameters obtained from the different methods indicated above, and with a summit identification (SID) model.

**2.1 Numerically Generated Rough Surfaces.** Isotropic rough surfaces consisting of 512 by 512 data points were generated with a sampling interval of  $dx = dy = 1 \mu\text{m}$  in both  $x$  and  $y$  direction. Sections of 256 by 256 points of three different types of these rough surfaces are shown in Fig. 1. Three different types of surfaces were generated with an exponential autocorrelation function with autocorrelation length of  $\beta^* = 10 \mu\text{m}$  [surface 1, Fig. 1(a)],  $20 \mu\text{m}$  [surface 2, Fig. 1(b)], and  $50 \mu\text{m}$  [surface 3, Fig. 1(c)], respectively. The surfaces are made of steel with a Young's modulus  $E = 210 \text{ GPa}$ , hardness  $H = 1.96 \text{ GPa}$ , and a Poisson's ratio  $\nu = 0.3$ . The  $Str$  parameter is used to describe the level of isotropy of a rough surface, which is defined as the ratio of the shortest and longest decay length of the two-dimensional autocorrelation function of that surface to a specified limit ( $s = 0.2$ ) [35,36]. A ratio of 1 ( $Str = 1$ ) indicates a perfectly isotropic surface. The values of the  $Str$  parameter of the rough surfaces used in this analysis were found to be 0.85 [surface 1, Fig. 1(a)], 0.92 [surface 2, Fig. 1(b)], and 0.96 [surface 3, Fig. 1(c)], respectively. The contact of two rough surfaces with identical autocorrelation function is then replaced by that of an equivalent rough surface and a rigid flat [3,14], after which the topography parameters of the equivalent surface are determined.

**2.2 Surface Topography Parameters Calculation.** Three methods that are commonly used in the literature to calculate the surface topography parameters are evaluated in the present study. The sampling interval and nominal contact area are identical for each method and equal to the corresponding values of the numerically generated surface (Fig. 1).

**2.2.1 Spectral Moments Approach Applied to a Single Arbitrary Cross Section.** The first method relies on determining the spectral moments  $m_0$ ,  $m_2$ , and  $m_4$  from a single arbitrary cross section of an isotropic rough surface using the approach developed by McCool [14]

$$m_0 = \text{AVG}[z^2] \quad (1)$$

$$m_2 = \text{AVG}\left[\left(\frac{dz}{dx}\right)^2\right] \quad (2)$$

$$m_4 = \text{AVG}\left[\left(\frac{d^2z}{dx^2}\right)^2\right] \quad (3)$$

where the AVG operator computes the arithmetic average, and  $z(x)$  is the surface height profile of an arbitrary cross section

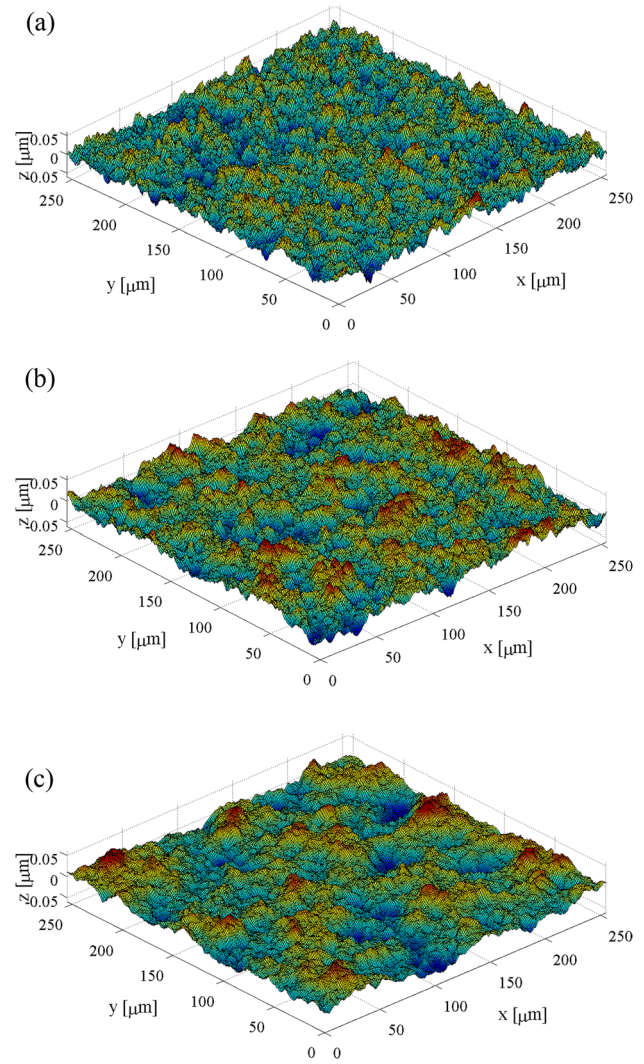


**Fig. 1** 256 by 256 point sections of the 512 by 512 point rough surfaces, (a) surface 1, (b) surface 2, and (c) surface 3

(trace) taken along the  $x$  direction of the 3D equivalent rough surface. The topography parameters  $\eta$ ,  $\rho$ , and  $\sigma_s$  are obtained from the spectral moments [Eqs. (1)–(3)] as

$$\eta = \left(\frac{m_4}{m_2}\right) / 6\pi\sqrt{3} \quad (4)$$

$$\rho = 0.375(\pi/m_4)^{\frac{1}{2}} \quad (5)$$

$$\sigma_s = \left(1 - \frac{0.8968}{\alpha}\right)^{\frac{1}{2}} m_0^{\frac{1}{2}} \quad (6)$$

where  $\alpha = (m_0 m_4) / m_2^2$  is the so-called bandwidth parameter. When this spectral moments approach is used, the values of  $\eta$ ,  $\rho$ , and  $\sigma_s$  for different arbitrary cross sections may vary considerably [13]. Furthermore, the topography parameters calculated from the spectral moments approach significantly depend on the finite difference discretization used to calculate the derivatives in Eqs. (2) and (3) [8,27]. While several schemes can be used, and the results obtained with different schemes can be related to each other [8], central finite difference discretization was used throughout this work for consistency.

**2.2.2 Spectral Moments Approach Averaged Over a Discrete Number of Cross Sections.** In the second method, the spectral moments are determined for all individual 512 cross sections

along the  $x$  direction of the equivalent rough surface using the approach described in Sec. 2.2.1. The average spectral moments are calculated and used to compute the corresponding topography parameters  $\eta$ ,  $\rho$ , and  $\sigma_s$ .

**2.2.3 Summit Identification Method.** Finally, a third method to find the surface topography parameters is based on determining the summits of the surface as local maxima using an 8-nearest neighbor summit identification scheme. The standard deviation of asperity heights  $\sigma_s$  is calculated from the  $n$  asperity heights and the asperity density  $\eta = n/A_n$ , with  $n$  the number of asperities (identical to the number of summits identified) and  $A_n$  the nominal surface area. To find the average asperity summit radius, the summit curvature is determined for each summit  $i$  in two orthogonal directions  $\kappa_{x,i} = d^2z/dx^2$  and  $\kappa_{y,i} = d^2z/dy^2$ , after which the radius of curvature  $\rho_i$  of that summit is computed as the inverse of the average of its  $\kappa_x$  and  $\kappa_y$ , i.e.,  $\rho_i = -[(\kappa_{x,i} + \kappa_{y,i})/2]^{-1}$  [7]. The mean summit radius  $\rho$  is calculated as the arithmetic mean of all individual summit radii.

**2.3 Comparison of the Different Methods to Determine the Surface Topography Parameters.** The resulting topography parameters for the equivalent rough surface are obtained using the three different methods described in Sec. 2.2, and summarized in Table 1 together with the dimensionless roughness parameter  $\beta$  (where  $\beta = \eta\rho\sigma_s > 1.93 \times 10^{-2}$  [37]), the plasticity index  $\psi$ , and the bandwidth parameter  $\alpha$ . For the method based on spectral moments of a single cross section, the maximum and minimum values of the topography parameters obtained from 512 cross sections in the  $x$  direction are presented, to indicate the range of results that can be obtained when determining  $\eta$ ,  $\rho$ , and  $\sigma_s$  for a 3D surface from the spectral moments of a single arbitrary cross section. Each extremum can belong to a different cross section. Additionally, the variation  $\Delta$  between the maximum and minimum value of each parameter is shown as a percentage of the minimum value. The bandwidth parameter  $\alpha = (m_0m_4)/m_2^2$  is only relevant to the spectral moments approach and is not calculated for the summit identification method.

From Table 1 it is observed that, when determined from an arbitrary cross section, the asperity density, mean asperity radius, and the standard deviation of asperity heights vary significantly between the minimum and maximum values. Furthermore, the values of  $\sigma_s$  and  $\rho$  obtained by using the summit identification

(SID) method fall within the range of the corresponding values determined from an arbitrary cross section. The difference between  $\sigma_s$  and  $\rho$  obtained from the SID method and the average spectral moment method is less than 15%, for each of the surfaces evaluated. However, the asperity density obtained with the SID method is significantly smaller than that for any arbitrary cross section, or the average spectral moment approach. This interesting observation can possibly result from overestimating the number of asperity summits with the spectral moment method. The mean value of the correlation coefficient between surface heights of neighboring points of the equivalent rough surface used in this work was verified as  $\exp(-dx/\beta^*)$  [38] to be approximately 0.90 for surface 1, 0.95 for surface 2, and 0.98 for surface 3, and it is noted that the difference between  $\eta$  and the other topography parameters obtained with the SID method and the average spectral moments method decreases with increasing correlation between neighboring points. Table 2 summarizes the extreme and average values of the spectral moments of all 512 cross sections in  $x$  and  $y$  directions, obtained for the equivalent rough surfaces derived from the three surfaces shown in Fig. 1. Additionally, the variation  $\Delta = (m_{i,\max} - m_{i,\min})/m_{i,\min}$  between the maximum and minimum value of each of the spectral moments  $m_i$  is presented in Table 2.

From Table 2 it is observed that the values of the spectral moments vary considerably for different cross sections of the surface (maximum versus minimum value). However, since the average values were found to be identical in both  $x$  and  $y$  directions (see Table 2), the surfaces may still be considered isotropic. Additionally, it is noted that the largest variation between the spectral moments of individual cross sections of the surface occurs for  $m_0$ , and that this variation increases with increasing autocorrelation length [ $\beta^*(\text{surface 3}) > \beta^*(\text{surface 2}) > \beta^*(\text{surface 1})$ ], which corresponds to the  $\sigma_s$  values observed in Table 1. These results indicate that over the nominal surface area, the surface height values  $z(x,y)$  used to calculate  $m_0$  are subject to more variation than the summit slope ( $m_2$ ) and curvature ( $m_4$ ).

### 3 Results and Discussion

**3.1 Comparison of the Contact Parameters Obtained From the GW Model and the Summit Identification Model.** In Sec. 3.1 the analysis is limited to contact of two rough surfaces of the type of surface 2, which has an autocorrelation length

**Table 1 Surface topography parameters calculated with different methods, sampling interval 1  $\mu\text{m}$**

Parameter	Spectral moments of arbitrary cross section: max. values	Spectral moments of arbitrary cross section: min. values	Percent variation between max. and min. values	Average spectral moments of 512 cross sections	Summit identification method (8-nearest neighbor)	
Surface 1	$\eta$ ( $1/\text{m}^2$ )	$11.66 \times 10^{10}$	$6.67 \times 10^{10}$	75%	$9.02 \times 10^{10}$	$3.31 \times 10^{10}$
	$\rho$ (m)	$1.00 \times 10^{-4}$	$0.80 \times 10^{-4}$	25%	$0.91 \times 10^{-4}$	$1.02 \times 10^{-4}$
	$\sigma_s$ (m)	$1.54 \times 10^{-8}$	$0.95 \times 10^{-8}$	62%	$1.24 \times 10^{-8}$	$1.16 \times 10^{-8}$
	$\psi$	0.78	0.59	32%	0.60	0.63
	$\beta$	$12.80 \times 10^{-2}$	$8.14 \times 10^{-2}$	57%	$10.06 \times 10^{-2}$	$3.90 \times 10^{-2}$
	$\alpha$	40.44	16.87	140%	25.55	N/A
	Surface 2	$\eta$ ( $1/\text{m}^2$ )	$9.92 \times 10^{10}$	$6.00 \times 10^{10}$	65%	$7.69 \times 10^{10}$
$\rho$ (m)		$1.47 \times 10^{-4}$	$1.13 \times 10^{-4}$	30%	$1.27 \times 10^{-4}$	$1.43 \times 10^{-4}$
$\sigma_s$ (m)		$1.66 \times 10^{-8}$	$1.00 \times 10^{-8}$	66%	$1.31 \times 10^{-8}$	$1.26 \times 10^{-8}$
$\psi$		0.68	0.52	31%	0.60	0.55
$\beta$		$17.79 \times 10^{-2}$	$9.29 \times 10^{-2}$	91%	$12.79 \times 10^{-2}$	$5.24 \times 10^{-2}$
$\alpha$		77.21	21.70	256%	40.83	N/A
Surface 3		$\eta$ ( $1/\text{m}^2$ )	$8.81 \times 10^{10}$	$5.18 \times 10^{10}$	70%	$6.77 \times 10^{10}$
	$\rho$ (m)	$2.24 \times 10^{-4}$	$1.80 \times 10^{-4}$	24%	$2.00 \times 10^{-4}$	$2.20 \times 10^{-4}$
	$\sigma_s$ (m)	$1.66 \times 10^{-8}$	$0.94 \times 10^{-8}$	77%	$1.29 \times 10^{-8}$	$1.27 \times 10^{-8}$
	$\psi$	0.55	0.40	38%	0.47	0.45
	$\beta$	$25.36 \times 10^{-2}$	$11.59 \times 10^{-2}$	119%	$17.43 \times 10^{-2}$	$7.28 \times 10^{-2}$
	$\alpha$	156.07	33.29	369%	75.38	N/A

**Table 2 Spectral moments**

		x direction				y direction			
		Maximum value	Minimum value	Average value	$\Delta(\%)$	Maximum value	Minimum value	Average value	$\Delta(\%)$
Surface 1	$m_0$	$2.42 \times 10^{-16}$	$0.94 \times 10^{-16}$	$1.60 \times 10^{-16}$	157	$2.45 \times 10^{-16}$	$0.98 \times 10^{-16}$	$1.60 \times 10^{-16}$	151
	$m_2$	$2.34 \times 10^{-5}$	$1.45 \times 10^{-5}$	$1.84 \times 10^{-5}$	62	$2.31 \times 10^{-5}$	$1.42 \times 10^{-5}$	$1.84 \times 10^{-5}$	63
	$m_4$	$6.85 \times 10^7$	$4.43 \times 10^7$	$5.39 \times 10^7$	55	$6.79 \times 10^7$	$4.41 \times 10^7$	$5.40 \times 10^7$	54
Surface 2	$m_0$	$2.79 \times 10^{-16}$	$1.05 \times 10^{-16}$	$1.77 \times 10^{-16}$	166	$2.98 \times 10^{-16}$	$1.01 \times 10^{-16}$	$1.77 \times 10^{-16}$	195
	$m_2$	$1.36 \times 10^{-5}$	$0.84 \times 10^{-5}$	$1.09 \times 10^{-5}$	61	$1.36 \times 10^{-5}$	$0.80 \times 10^{-5}$	$1.09 \times 10^{-5}$	70
	$m_4$	$3.48 \times 10^7$	$2.05 \times 10^7$	$2.74 \times 10^7$	70	$3.40 \times 10^7$	$2.21 \times 10^7$	$2.74 \times 10^7$	54
Surface 3	$m_0$	$2.79 \times 10^{-16}$	$0.91 \times 10^{-16}$	$1.70 \times 10^{-16}$	206	$3.12 \times 10^{-16}$	$0.75 \times 10^{-16}$	$1.70 \times 10^{-16}$	316
	$m_2$	$0.64 \times 10^{-5}$	$0.40 \times 10^{-5}$	$0.50 \times 10^{-5}$	58	$0.63 \times 10^{-5}$	$0.37 \times 10^{-5}$	$0.50 \times 10^{-5}$	67
	$m_4$	$1.36 \times 10^7$	$0.88 \times 10^7$	$1.10 \times 10^7$	54	$1.39 \times 10^7$	$0.90 \times 10^7$	$1.10 \times 10^7$	54

( $\beta^* = 20 \mu\text{m}$ ) in between that of surfaces 1 and 3. Using the GW model, the number of contacting asperities  $n_p$ , the nondimensional real area of contact  $A^* = A_r/A_n$ , and the nondimensional normal load  $P^* = P/A_n E'$  are calculated as a function of the nondimensional separation  $d^* = d/\sigma_s$  between the equivalent rough surface and a rigid flat [1].

$$n_p = \eta A_n \int_{d^*}^{\infty} \Phi(z^*) dz^* \quad (7)$$

$$A^* = \pi \beta \int_{d^*}^{\infty} (z^* - d^*) \Phi(z^*) dz^* \quad (8)$$

$$P^* = \frac{4}{3} \rho^2 \sigma_s^3 \eta \int_{d^*}^{\infty} (z^* - d^*)^2 \Phi(z^*) dz^* \quad (9)$$

Here

$$\Phi(z^*) = \frac{1}{\sqrt{2\pi}} e^{-\frac{1}{2} z^{*2}}$$

is the nondimensional Gaussian probability density function of surface heights.

The relationship between the nondimensional separation based on surface heights  $h^*$  and the nondimensional separation based on asperity heights  $d^*$  is depicted in Fig. 2, and is given by  $h^* = d^* + y^*$ , where  $y^* = [4(m_0/\pi\alpha)^{1/2}]/\sigma_s$  [39].

The GW model is evaluated using topography parameters  $\eta$ ,  $\rho$ , and  $\sigma_s$  obtained with the three different methods described in Sec. 2.2. In the following results, the spectral moments method applied to an arbitrary cross section is represented by the envelope bound by the upper extreme case (GW upper extreme model) and the lower extreme case (GW lower extreme model), for any specific contact parameter. The result from a single arbitrary cross section, which may vary significantly as shown in Table 1, will fall within this envelope. Hence, the GW lower and upper extreme boundaries describe and quantify the worst case scenarios. Results for the GW model with topography parameters obtained from the average spectral moment values (GW average model) and the

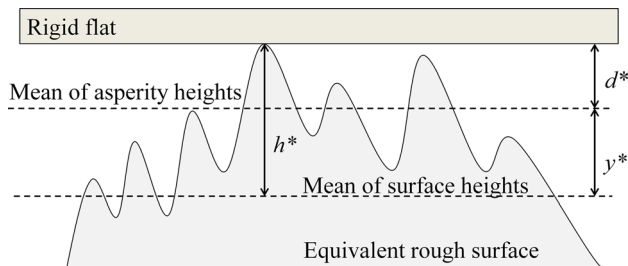


**Fig. 2 Equivalent rough surface and rigid flat**

summit identification scheme (GW w/SID model) are also obtained. A comparison is made with the results obtained from the summit identification scheme (SID model). In the latter method, all asperities of the equivalent rough surface are identified using an 8-nearest neighbor scheme, and the contribution to the nondimensional real area of contact  $A^*$  [Eq. (10)] and the normal load  $P^*$  [Eq. (11)] of each individual contacting asperity is calculated and summed:

$$A^* = \frac{\pi \rho \sigma_s}{A_n} \sum_{i=1}^{n_p} (z_i^* - d^*) \quad (10)$$

$$P^* = \frac{4}{3} \frac{\rho^2 \sigma_s^3}{A_n} \sum_{i=1}^{n_p} (z_i^* - d^*)^2 \quad (11)$$

The results in this work are evaluated over the range  $0 \leq h^* \leq 3$ . It is assumed that practically no contact exists between the equivalent rough surface and the rigid flat when  $h^* > 3$  [40]. According to Kogut and Etsion [37] bulk deformation may occur when  $P^* > 10^{-3}$ , which in this work corresponds to approximately  $h^* = 0$ . As a result of bulk deformation, individual asperities may interact and/or be compressed together, which violates one of the GW model assumptions.

The SID model is assumed to provide the most reliable results compared to the other models discussed in this paper. The SID surface topography parameters are derived from the entire 3D surface and the actual asperities, as opposed to using statistical analysis based on limited data, i.e., a discrete number of cross sections. Moreover, the number of contacting asperities is determined exactly (also at large separations), and the contribution of each contacting asperity is summed to yield the total value of the real area of contact and normal load. Hence, in the following, the deviation between the different models is quantified by comparing the results for each model relative to those obtained with the SID model. The deviation between the different models and the SID model is hereafter referred to as the error with respect to the SID model.

Figure 3(a) shows the number of contacting asperities  $n_p$ , and Fig. 3(b) shows the percent error of the number of contacting asperities versus the nondimensional separation based on surface heights  $h^*$ , respectively.

From Fig. 3(a) it is observed that the number of contacting asperities as a function of  $h^*$  predicted by the different models varies significantly, except for the SID and the GW with SID topography parameters (GW w/SID) models, which result in the lowest values of  $n_p$ . Since each model in Fig. 3(a) uses different topography parameters—in particular the asperity density and the standard deviation of asperity heights (see Table 1)—a different number of contacting asperities is found for each model for a given nondimensional separation  $h^*$ . The SID and GW with SID topography parameters models; on the other hand, use identical

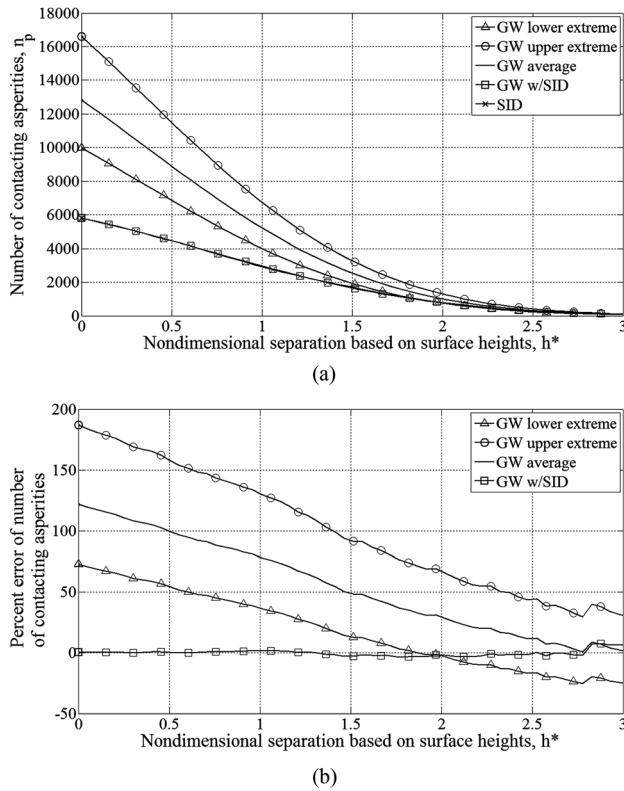


**Fig. 3 (a) Number of contacting asperities and (b) percent error of the number of contacting asperities versus nondimensional separation based on surface heights**

values of the topography parameters, namely the ones obtained with the SID method and hence, they seem to overlap. The different models diverge with decreasing separation because more asperities come into contact, which emphasizes the effect of the different asperity density in each model. Figure 3(b) shows quantitatively how much the results from the different models deviate from the SID model. The deviation varies between  $-26\%$  and  $187\%$  for the extreme cases where the surface topography parameters were derived from a single cross section of the rough surface. The error committed by using the GW model with surface topography parameters obtained from a single cross section of the equivalent rough surface may be significant depending on the arbitrary cross section used. The actual error will be contained within the envelope bound by the lower and upper extreme errors in Fig. 3(b).

The number of contacting asperities for a given separation depends on  $\eta$  and  $\sigma_s$ . While the lowest  $\eta$  value was found for the SID method (and used in the SID model), a negative error of the number of contacting asperities is observed for  $h^* > 1.5$  in the GW lower extreme case, i.e., the number of contacting asperities is underestimated. Each cross section is characterized by a different  $\sigma_s$  value, and the maximum value is approximately 30% larger than the  $\sigma_s$  value obtained with the SID method (see Table 1). A single cross section can thus show a smaller number of contacting asperities than the SID model, despite the larger  $\eta$  value. In the case of the GW model with topography parameters based on average spectral moments (GW average), the error of the number of contacting asperities is 120% at  $h^* = 0$ , and it decreases to approximately 10% at  $h^* = 3$ .

Figure 4(a) depicts the nondimensional real area of contact  $A^*$  and Fig. 4(b) depicts the percent error of the real area of contact as a function of the nondimensional separation based on surface heights  $h^*$ , respectively. Since the real area of contact is directly related to the number of contacting asperities and the contact area per asperity, the same observations are made as in Fig. 3, i.e., the

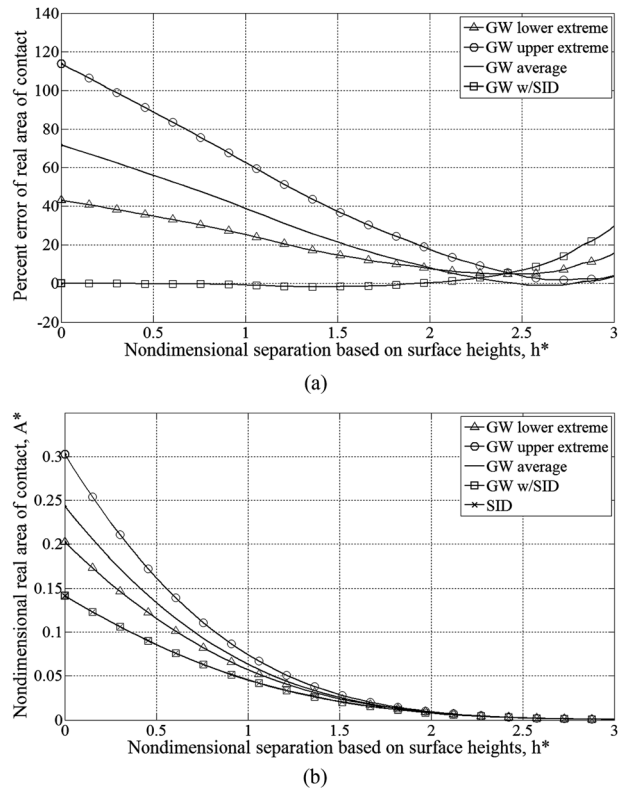


**Fig. 4 (a) Nondimensional real area of contact and (b) percent error of real area of contact versus nondimensional separation based on surface heights**

lowest values of the nondimensional real area of contact are obtained for the models based on the SID topography parameters, and the models diverge with decreasing separation.

Figure 5(a) shows the nondimensional separation based on surface heights  $h^*$  and Fig. 5(b) the percent error of the nondimensional separation as a function of the nondimensional normal load  $P^*$ , respectively. While the different models result in a different separation for a given nondimensional normal load, it is noted that the GW with SID topography parameters and the SID models overlap for  $0 < h^* < 2$ . For  $h^* > 2$ , these two models diverge; as a result of the different treatment of contacting asperities in the SID model (discrete) as opposed to the GW model (continuous), which is discussed in greater detail at the end of Sec. 3.1. From Figs. 4(b) and 5(b) it is observed that the error committed by using the SID topography parameters in the GW model yields the smallest percent errors compared to the SID model. Furthermore, from Fig. 5(b) it is observed that the error for the case of the GW extreme and average models approaches infinity when the load increases ( $h^*$  decreases) since the error is calculated relative to the SID model. When  $h^*$  approaches zero in the SID model ( $P^*$  increases) the percent error  $(h_{GW}^* - h_{SID}^*)/h_{SID}^*$  approaches infinity, regardless of the absolute error value, even with negligible differences of  $h^*$  compared to the SID model. The error becomes finite again for negative values of  $h^*$ . However, no negative values of  $h^*$  are considered in this work. The smallest error is observed for the GW with SID parameters model. Hence, Fig. 5(b) should be used with caution since the results may be misleading at high  $P^*$  values.

The numerical values of the maximum and minimum percent errors obtained from Figs. 3(b), 4(b), and 5(b) are summarized in Table 3 for the different models. From Table 3 it is again observed that the GW with SID model results in the smallest error interval. Moreover, it is important to point out that in the case of the GW with SID topography parameters model the largest error values occur at  $h^* = 3$ . Thus, the errors committed with the GW with

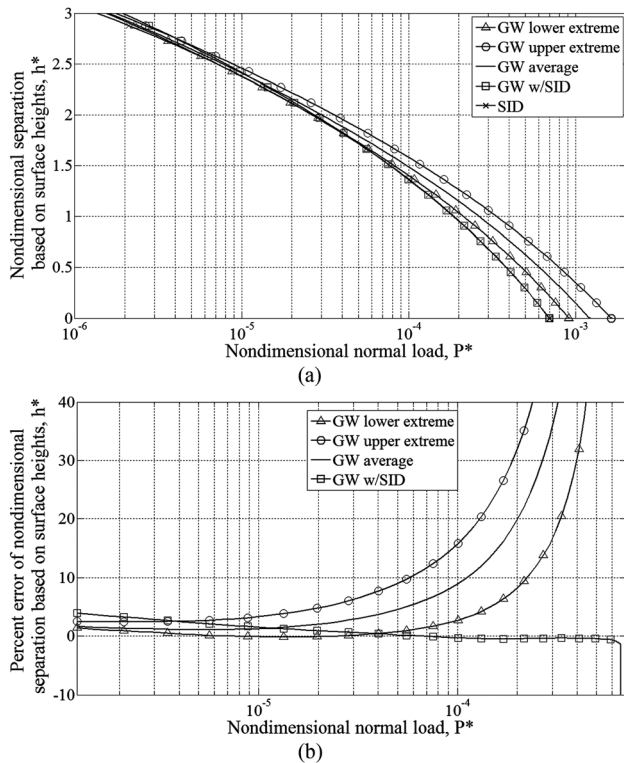


**Fig. 5 (a) Nondimensional separation based on surface heights and (b) percent error of the nondimensional separation based on surface heights versus nondimensional normal load**

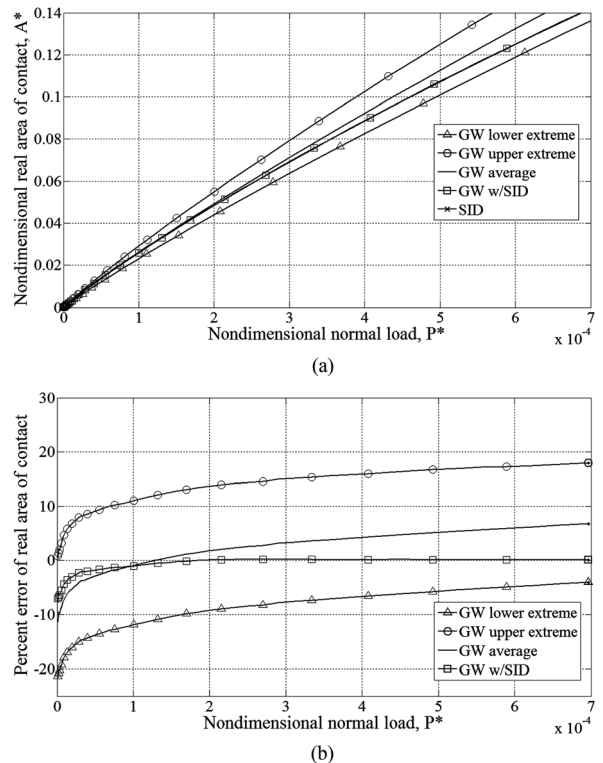
SID model for any  $h^* < 2.5$  are in fact much lower than the maximum values shown in Table 3.

Figure 6(a) displays the nondimensional real area of contact  $A^*$ , while Fig. 6(b) shows the percent error of  $A^*$  versus the nondimensional normal load  $P^*$ , respectively. The data are shown for  $A^* \leq 0.14$  since this upper limit coincides with  $h^* = 0$  for the SID model, and no negative values for  $h^*$  were considered in this study. Furthermore, the load was limited to  $P^* = 7.0 \times 10^{-4}$  since at this load the separation becomes  $h^* = 0$  in the SID model.

The differences between the contact parameters predicted by the different models, depicted in Figs. 3–6, result from two main reasons. At small separations ( $0 < h^* < 2$ ), it is the different asperity density  $\eta$  used in the GW and SID models that plays the most important role, which is anticipated, as the asperity density appears in Eqs. (7)–(9). It also affects the summations over the number of contacting asperities, which indirectly depends on the asperity density, in Eqs. (10) and (11). At large separations ( $h^* > 2$ ) the different treatment of the number of contacting asperities is the dominant factor. In the SID model, the asperities (summits) in contact with the rigid flat are identified individually and their contribution to the normal load and real contact area is calculated and summed. A discrete number of asperities makes contact, and above a certain finite separation  $h^*$ , no asperities remain in contact. In the GW with SID topography parameters model, a

**Table 3 Percent error value**

Model	Error interval $n_p$ (%)		Error interval $A_r/A_n$ (%)		Error interval $h/\sigma_s$ (%)	
GW lower extreme	-25.74	72.40	4.88	43.06	-0.14	$\infty$
GW upper extreme	29.56	186.86	1.79	113.67	2.41	$\infty$
GW average	0.61	121.77	-1.06	71.74	1.10	$\infty$
GW w/SID	-3.64	7.35	-1.70	32.51	$\infty$	3.91



**Fig. 6 (a) Nondimensional real area of contact and (b) percent error of the real area of contact versus nondimensional normal load**

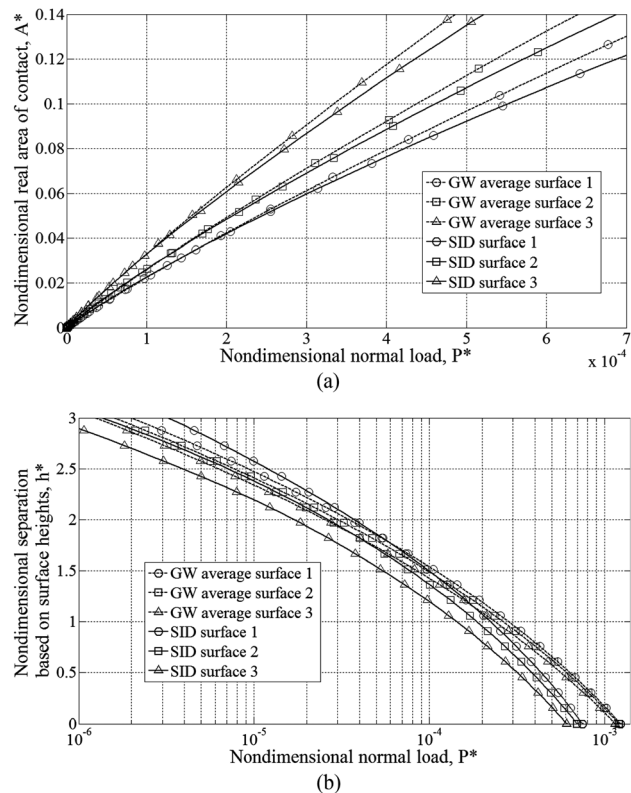


**Fig. 7 (a) Nondimensional real area of contact and (b) nondimensional separation based on surface heights versus nondimensional normal load**

**Table 4 Percent error values for different surfaces and models**

Model		Error interval $n_p$ (%)		Error interval $A_r/A_n$ (%)		Error interval $h/\sigma_s$ (%)	
Surface 1	GW lower extreme	-42.55	66.77	-31.69	47.82	-5.94	$\infty$
	GW upper extreme	-7.63	177.89	-43.89	88.96	-3.79	$\infty$
	GW average	-29.64	120.80	-39.72	64.44	-5.11	$\infty$
	GW w/SID	-1.92	6.81	-0.36	3.63	$\infty$	0.61
Surface 2	GW lower extreme	-25.74	72.40	4.88	43.06	-0.14	$\infty$
	GW upper extreme	29.56	186.86	1.79	113.67	2.41	$\infty$
	GW average	0.61	121.77	-1.06	71.74	1.10	$\infty$
	GW w/SID	-3.64	7.35	-1.70	32.51	$\infty$	3.91
Surface 3	GW lower extreme	9.61	78.98	29.25	66.60	3.39	$\infty$
	GW upper extreme	62.20	188.95	62.32	147.94	7.38	$\infty$
	GW average	39.58	127.46	38.95	87.25	5.72	$\infty$
	GW w/SID	-5.25	31.12	-0.79	44.27	$\infty$	4.68

statistical approach is used that calculates the number of contacting asperities based on a Gaussian distribution of asperity heights. Thus, while in the SID model a discrete number of asperities makes contact and zero normal load and real contact area are achieved above a certain finite separation, the GW model overestimates the number of asperities in contact at large separations because  $n_p \rightarrow 0$  when  $h^* \rightarrow \infty$ . Consequently, for large values of  $h^*$ , the SID model predicts smaller values for the contact parameters than the GW with SID topography parameters model, as is for instance shown in Fig. 5(a).

**3.2 Effect of the Autocorrelation Length.** The autocorrelation length of the different surfaces is  $\beta^* = 10 \mu\text{m}$  [surface 1, Fig. 1(a)],  $20 \mu\text{m}$  [surface 2, Fig. 1(b)], and  $50 \mu\text{m}$  [surface 3, Fig. 1(c)]. The sampling interval was kept constant at  $1 \mu\text{m}$  for all surfaces and results discussed in Sec. 3.2. Figure 7(a) shows the nondimensional real area of contact  $A^*$  and Fig. 7(b) shows the nondimensional separation based on surface heights  $h^*$  as a function of the nondimensional normal load  $P^*$ , respectively. Only the results for the GW average model and the SID model are shown for clarity.

It is expected that different  $A^*$  versus  $P^*$  and  $h^*$  versus  $P^*$  curves are obtained for surfaces with a different autocorrelation length. For a constant  $P^*$ , the smoothest surface (surface 3) will result in the largest  $A^*$  [Fig. 7(a)] and, correspondingly, the smallest  $h^*$  [Fig. 7(b)]. Table 4 shows a comparison between the extreme deviations of the different contact parameters obtained with the four different models, relative to the SID model, for each of the three different rough surfaces considered in this work. These deviations are determined from the results shown in Fig. 7, in addition to the results for GW upper and lower extreme, and GW with SID, not displayed in Fig. 7.

Identical to Fig. 5(b) and Table 3, it is observed that the error  $(h_{GW}^* - h_{SID}^*)/h_{SID}^*$  may approach infinity when  $h^*$  approaches zero in the SID model ( $P^*$  increases). Furthermore, it is noted that for all contact parameters, the error obtained for the GW average model is contained within the interval bound by the results of the GW lower and upper extreme models. Both the lower and upper limit of the error of  $n_p$ ,  $A_r/A_n$ , and  $h/\sigma_s$  increase with increasing autocorrelation length.

**3.3 Effect of the Sampling Interval.** Figure 8 shows the nondimensional separation based on surface heights  $h^*$  as a function of the nondimensional normal load  $P^*$ , for three different sampling intervals 1, 2, and  $3 \mu\text{m}$ , for (a) surface 1, (b) surface 2, and (c) surface 3. The sampling interval is limited to three times the original sampling interval of  $1 \mu\text{m}$ . When increasing the sampling interval while keeping the nominal surface area constant, the number of points describing the surface is reduced. Again, only the results for the GW average model and the SID model are shown for clarity. It is observed that at  $h^* = 3$  the difference

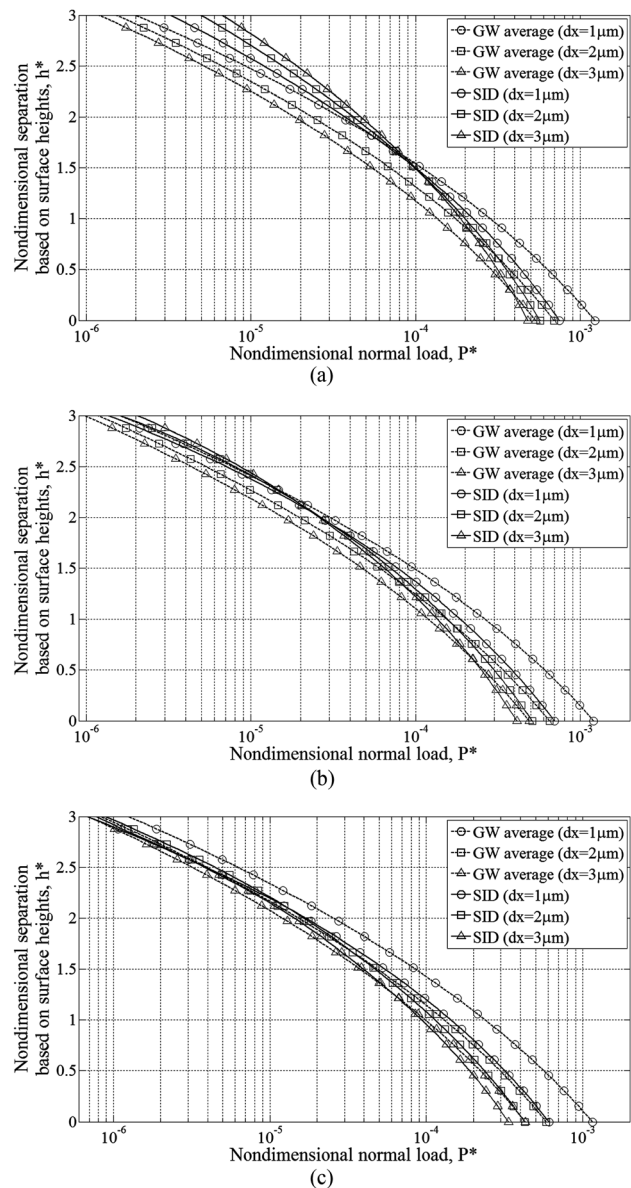


**Fig. 8 Nondimensional separation based on surface heights versus nondimensional normal load for (a) surface 1, (b) surface 2, and (c) surface 3**

**Table 5 Topography parameters of surface 2, obtained for a sampling interval of 2 and 3  $\mu\text{m}$**

Sampling length	Parameter	Spectral moments of arbitrary cross section: max. values	Spectral moments of arbitrary cross section: min. values	Average spectral moments of 512 cross sections	Summit identification method (8-nearest neighbor)
2 $\mu\text{m}$	$\eta$ ( $1/\text{m}^2$ )	$2.98 \times 10^{10}$	$1.69 \times 10^{10}$	$2.24 \times 10^{10}$	$1.09 \times 10^{10}$
	$\rho$ (m)	$3.64 \times 10^{-4}$	$2.66 \times 10^{-4}$	$3.11 \times 10^{-4}$	$3.54 \times 10^{-4}$
	$\sigma_s$ (m)	$1.65 \times 10^{-8}$	$0.97 \times 10^{-8}$	$1.30 \times 10^{-8}$	$1.21 \times 10^{-8}$
	$\psi$	0.45	0.32	0.38	0.34
	$\beta$	$12.67 \times 10^{-2}$	$6.31 \times 10^{-2}$	$9.00 \times 10^{-2}$	$4.69 \times 10^{-2}$
	$\alpha$	39.63	10.51	20.72	N/A
3 $\mu\text{m}$	$\eta$ ( $1/\text{m}^2$ )	$1.78 \times 10^{10}$	$0.84 \times 10^{10}$	$1.28 \times 10^{10}$	$0.62 \times 10^{10}$
	$\rho$ (m)	$6.10 \times 10^{-4}$	$4.23 \times 10^{-4}$	$5.09 \times 10^{-4}$	$5.91 \times 10^{-4}$
	$\sigma_s$ (m)	$1.65 \times 10^{-8}$	$0.98 \times 10^{-8}$	$1.29 \times 10^{-8}$	$1.17 \times 10^{-8}$
	$\psi$	0.35	0.25	0.30	0.26
	$\beta$	$12.46 \times 10^{-2}$	$6.08 \times 10^{-2}$	$8.31 \times 10^{-2}$	$4.30 \times 10^{-2}$
	$\alpha$	38.37	9.83	17.82	N/A

between the results for the SID and GW average model is maximum for the largest sampling interval (3  $\mu\text{m}$ ), while at  $h^* = 0$  the difference between the results for the SID and GW average model is maximum for the smallest sampling interval (1  $\mu\text{m}$ ). Furthermore, it is noticed from Figs. 8(a), 8(b), and 8(c) that for increasing autocorrelation length the differences in  $h^*$  obtained with the SID and GW average model decrease, in particular at large separations.

Table 5 supplements Table 1, and shows the topography parameters obtained with the three different methods, for a sampling interval of 2 and 3  $\mu\text{m}$ , for surface 2 only. Since the results in Sec. 3.1 were obtained for surface 2, this allows for comparison. It is observed that for all methods the asperity density decreases, and the mean summit radius increases for increasing sampling interval, which is in agreement with the results from [26,38,41]. Table 5 presents the topography parameters obtained from surface 2, for a sampling interval of 2 and 3  $\mu\text{m}$ . Additionally, the topography parameters were obtained for all three surfaces for the three different sampling intervals. It was found that with increasing sampling

interval the change in topography parameters was minimum for surface 3. This is the smoothest surface because it has the largest autocorrelation length and the largest mean asperity radius of the three surfaces considered. Hence, when the sampling interval is increased, the same asperities are detected for surfaces with a large mean asperity radius, as compared to surfaces with a smaller mean asperity radius.

Using the topography parameters obtained for all three surfaces for sampling intervals of 2 and 3  $\mu\text{m}$ , respectively, the resulting contact parameters are calculated. Together with Tables 4, and 6 shows a comparison between the extreme errors of the different contact parameters obtained with the four different models, relative to the SID model, for each of the three different rough surfaces considered in this work, and for a sampling interval of 1  $\mu\text{m}$  (Table 4), 2  $\mu\text{m}$  [Table 6(a)], and 3  $\mu\text{m}$  [Table 6(b)].

From Tables 4 and 6 it is observed that contact parameters obtained from surface 3 are least affected by using a different sampling interval, irrespective of the method used to determine the topography parameters. This was expected since the

**Table 6 Percent error values for different surfaces and models, sampling interval (a) 2  $\mu\text{m}$  and (b) 3  $\mu\text{m}$**

Model		Error interval $n_p$ (%)		Error interval $A_s/A_n$ (%)		Error interval $h/\sigma_s$ (%)	
(a) Surface 1	GW lower extreme	-71.25	32.92	-58.70	7.92	$\infty$	-13.29
	GW upper extreme	-56.37	131.06	-75.73	36.97	-13.42	$\infty$
	GW average	-61.93	71.76	-70.81	21.20	$\infty$	-13.29
	GW w/SID	-1.91	7.47	-4.73	2.05	$\infty$	0.43
Surface 2	GW lower extreme	-54.09	30.00	-26.23	7.79	-8.35	$\infty$
	GW upper extreme	-26.46	117.80	-47.51	51.78	-5.00	$\infty$
	GW average	-43.78	69.49	-41.83	25.4	-6.42	$\infty$
	GW w/SID	-6.68	1.94	-0.97	31.77	$\infty$	4.81
Surface 3	GW lower extreme	-32.24	23.34	-6.25	9.13	$\infty$	0.33
	GW upper extreme	3.54	130.30	-19.92	74.05	-0.23	$\infty$
	GW average	-20.08	70.34	-19.01	35.36	-1.93	$\infty$
	GW w/SID	-9.23	14.84	-2.83	18.28	$\infty$	2.80
(b) Surface 1	GW lower extreme	-78.68	19.88	-74.34	-3.17	$\infty$	-19.52
	GW upper extreme	-74.38	132.96	-86.30	30.78	-19.78	$\infty$
	GW average	-76.75	69.11	-83.01	9.76	-21.61	$\infty$
	GW w/SID	-2.17	4.01	-6.07	0.67	-1.25	46.83
Surface 2	GW lower extreme	-63.20	13.79	-46.24	3.40	-13.10	$\infty$
	GW upper extreme	-41.46	123.70	-66.38	45.99	-10.92	$\infty$
	GW average	-56.06	64.54	-59.73	16.97	-10.96	$\infty$
	GW w/SID	-8.37	1.68	-1.17	12.63	$\infty$	2.85
Surface 3	GW lower extreme	-49.80	22.39	-7.52	31.28	$\infty$	0.98
	GW upper extreme	-6.36	133.72	-28.00	49.80	-1.60	$\infty$
	GW average	-29.25	67.51	-26.60	24.83	-3.57	$\infty$
	GW w/SID	-14.58	43.71	-1.20	45.14	$\infty$	4.10

topography parameters change least with increasing sampling interval for surface 3, independent of the method used to determine them.

#### 4 Conclusion

A quantitative analysis of the different results obtained when calculating the relationship between the number of contacting asperities, the separation, the real area of contact, and the normal load, using different methods to determine the asperity density  $\eta$ , summit radius  $\rho$ , and standard deviation of asperity heights  $\sigma_s$  of a 3D isotropic rough surface was provided. Thereto, the topography parameters for computer generated isotropic rough surfaces were obtained with the spectral moments method, and were compared to the corresponding parameters obtained by a summit identification method using an 8-nearest neighbor scheme. Likewise, the contact parameters of the GW model were compared to the corresponding parameters of the summit identification model. The effect of the autocorrelation length and the sampling interval were investigated.

The topography parameters obtained from a single arbitrary cross section of an actual isotropic 3D rough surface using the spectral moments method vary significantly depending on which cross section is selected. Hence, this method is not reliable to determine the topography parameters of an actual isotropic 3D rough surface. An approach that results in a unique solution is to average the various spectral moments obtained from a set of many single cross sections and calculate the topography parameters from these average values. For the actual isotropic 3D equivalent rough surface used in this paper, the average spectral moments for 512 cross sections in the  $x$  and  $y$  direction, respectively, were found to be identical.

The main cause of the potentially large error of the contact parameters when using topography parameters determined from a single arbitrary cross section of the 3D equivalent rough surface originates from the large variation of the asperity density between different arbitrary cross sections. Additionally, the asperity density is the main difference between the topography parameters obtained using the spectral moments method and the summit identification method. It was found to be significantly smaller for the summit identification method than for the average spectral moment method, for the specific isotropic equivalent rough surfaces analyzed in this work.

As a result of the different topography parameters obtained with each method, the relationship between the number of contacting asperities, the real area of contact, and the normal load vary substantially for the GW and SID models. In the latter model the contact parameters are determined from the actual surface rather than based on a statistical approach. This seems to be more reliable as it includes all available information of the surface rather than relying on a discrete number of cross sections. The GW model with topography parameters obtained with the SID method (GW w/SID) seems to be the better choice among all the other GW model options that are considered in this work for realistic 3D isotropic rough surfaces. While an SID method may at first seem impractical for characterization of surface topography parameters, it is pointed out that white light interferometers for instance, allow digitizing a 3D surface roughness profile, which then enables using a summit identification scheme. The main cause of the error of the various contact parameters compared to the SID model is twofold. At small separations ( $0 < h^* < 2$ ), the different asperity density  $\eta$  used in the GW and SID models is the most important factor, and at large separations ( $h^* > 2$ ), the different treatment of the number of contacting asperities is the dominant parameter. In the SID model no asperity makes contact above a specific finite separation. Hence, zero normal load and real contact area are obtained above that separation. The GW model overestimates the different contact parameters at large separations because  $n_p \rightarrow 0$  only when  $h^* \rightarrow \infty$ .

The effect of the autocorrelation on the resulting contact parameters obtained from the four different models was examined, and it was found that for increasing autocorrelation length, the resulting

contact parameters become less sensitive to the sampling interval, irrespective of the method to determine the topography parameters.

This paper presents a relative comparison of different methods to determine the topography parameters, and contact parameters obtained from different models. The nominal area of contact and the number of points that describe the surface were kept constant for all calculations. These parameters seem to influence the resulting topography values and hence, despite the controlled numerically generated surfaces, uncertainty about the exact values of the unique topography parameters of a 3D rough surface still remains, and needs to be addressed in future studies.

#### Nomenclature

- $A_n$  = nominal area of contact
- $A_r$  = real area of contact
- $A^*$  = nondimensional real area of contact,  $A_r/A_n$
- $E_{1,2}$  = Young's modulus of material 1 and 2
- $E'$  = equivalent Young's modulus,  $\left(\frac{1-\nu_1^2}{E_1} + \frac{1-\nu_2^2}{E_2}\right)^{-1}$
- $H$  = hardness of the softer material of the contact pair
- $P$  = normal load
- $P^*$  = nondimensional normal load,  $P/A_n E'$
- $d$  = separation based on asperity heights
- $dx$  = sampling interval in the  $x$  direction
- $dy$  = sampling interval in the  $y$  direction
- $d^*$  = nondimensional separation based on asperity heights,  $d/\sigma_s$
- $h$  = separation based on surface heights
- $h^*$  = nondimensional separation based on surface heights,  $h/\sigma$
- $m_{0,2,4}$  = spectral moments
- $n$  = number of asperities
- $n_p$  = number of contacting asperities
- $y^* = h^* - d^*$
- $z$  = surface heights
- $z^*$  = nondimensional surface heights,  $z/\sigma$

#### Greek

- $\Phi$  = probability density function of the normal distribution of surface heights
- $\Phi^*$  = nondimensional probability density function of the normal distribution,  $\Phi\sigma_s$
- $\Psi$  = plasticity index,  $\frac{E'}{H} \sqrt{\frac{\sigma_s}{\rho}}$
- $\alpha$  = bandwidth parameter,  $\frac{m_0 m_4}{m_2^2}$
- $\beta = \eta\rho\sigma_s$
- $\beta^*$  = autocorrelation length
- $\eta$  = asperity density
- $\kappa_{x,y}$  = asperity summit curvature in the  $x$  and  $y$  direction
- $\nu_{1,2}$  = Poisson's ratio of material 1 and 2
- $\rho$  = mean summit radius
- $\sigma$  = standard deviation of surface heights
- $\sigma_s$  = standard deviation of asperity heights

#### References

- [1] Greenwood, J. A., and Williamson, J. B. P., 1966, "Contact of Nominally Flat Surfaces," *Proc. R. Soc. A. Math. Phys.*, **295**, pp. 300–319.
- [2] Greenwood, J. A., and Tripp, J. H., 1967, "The Elastic Contact of Rough Spheres," *J. Appl. Mech.*, **34**(1), pp. 153–159.
- [3] Greenwood, J. A., and Tripp, J. H., 1970, "The Contact of Two Nominally Flat Surfaces," *Proc. Int. Mech. Eng.*, **185**, pp. 625–634.
- [4] Bush, A. W., Gibson, R. D., and Thomas, T. R., 1975, "The Elastic Contact of Rough Surface," *Wear*, **35**(1), pp. 87–111.
- [5] O'Callaghan, M., and Cameron, M., 1976, "Static Contact Under Load Between Nominally Flat Surfaces in Which Deformation Is Purely Elastic," *Wear*, **36**(1), pp. 79–97.
- [6] Greenwood, J. A., 2006, "A Simplified Elliptical Model for Rough Surface Contact," *Wear*, **261**(2), pp. 191–200.
- [7] Carbone, G., and Bottiglione, F., 2008, "Asperity Contact Theories: Do They Predict Linearity Between Contact Area and Load?" *J. Mech. Phys. Solids*, **56**(8), pp. 2555–2572.

- [8] Paggi, M., and Ciavarella, M., 2010, "The Coefficient of Proportionality  $\kappa$  Between Real Contact Area and Load, With New Asperity Models," *Wear*, **268**, pp. 1020–1029.
- [9] Carbone, G., and Bottiglione, F., 2011, "Contact Mechanics of Rough Surfaces: A Comparison Between Theories," *Meccanica*, **46**(3), pp. 557–565.
- [10] Majumdar, A., and Bhushan, B., 1991, "Fractal Model of Elastic–Plastic Contact Between Rough Surfaces," *ASME J. Tribol.*, **113**, pp. 1–11.
- [11] Persson, B. N. J., 2001, "Theory of Rubber Friction and Contact Mechanics," *J. Chem. Phys.*, **115**, 3840–3861.
- [12] McCool, J. I., 1986, "Comparison of Models for the Contact of Rough Surfaces," *Wear*, **107**(1), pp. 37–60.
- [13] McCool, J. I., 1986, "Predicting Microcontact in Ceramics Via a Microcontact Model," *ASME J. Tribol.*, **108**(3), pp. 380–386.
- [14] McCool, J. I., 1987, "Relating Profile Instrument Measurements to the Functional Performance of Rough Surfaces," *ASME J. Tribol.*, **109**(2), pp. 264–270.
- [15] Zhao, Y., and Chang, L., 2001, "A Model of Asperity Interactions in Elastic–Plastic Contact of Rough Surfaces," *ASME J.*, **123**(4), pp. 57–64.
- [16] Lee, C. H., and Polycarpou, A., 2007, "Static Friction Experiments and Verification of an Improved Elastic–Plastic Model Including Roughness Effects," *ASME J. Tribol.*, **129**(4), pp. 754–760.
- [17] Akbarzadeh, S., and Khonsari, M., 2008, "Performance of Spur Gears Considering Surface Roughness and Shear Thinning Lubricant," *ASME J. Tribol.*, **130**(2), p. 021503.
- [18] Uchidate, M., Iwabuchi, A., Kikuchi, K., and Shimizu, T., 2009, "Research on the Validity of Using Nayak's Theory for Summit Parameters of Discrete Isotropic Gaussian Surfaces," *J. Adv. Mech. Des. Syst. Manuf.*, **3**(2), pp. 125–135.
- [19] Wilson, W. E., Angadi, S. V., and Jackson, R. L., 2010, "Surface Separation and Contact Resistance Considering Sinusoidal Elastic–Plastic Multi-Scale Rough Surface Contact," *Wear*, **268**(1–2), pp. 190–201.
- [20] Lee, C. H., Eriten, M., and Polycarpou, A., 2010, "Application of Elastic–Plastic Static Friction Models to Rough Surfaces With Asymmetric Asperity Distribution," *ASME J. Tribol.*, **132**(3), p. 031602.
- [21] Dickey, R. D. I., Jackson, R., and Flowers, G., 2011, "Measurements of the Static Friction Coefficient Between Tin Surfaces and Comparison to a Theoretical Model," *ASME J. Tribol.*, **133**(3), p. 031408.
- [22] Kogut, L., and Jackson, R., 2006, "A Comparison of Contact Modeling Utilizing Statistical and Fractal Approaches," *ASME J. Tribol.*, **128**(1), pp. 213–217.
- [23] Etsion, I., and Amit, M., 1993, "The Effect of Small Normal Loads on the Static Friction Coefficient for Very Smooth Surfaces," *ASME J. Tribol.*, **115**(3), pp. 406–410.
- [24] Raeymaekers, B., Etsion, I., and Talke, F. E., 2007, "Enhancing Tribological Performance of the Magnetic Tape/Guide Interface by Laser Surface Texturing," *Tribol. Lett.*, **27**(1), pp. 89–95.
- [25] Jackson, R. L., and Green, I., 2011, "On the Modeling of Elastic Contact Between Rough Surfaces," *Tribol. T.*, **54**, pp. 300–314.
- [26] Greenwood, J. A., 1984, "A Unified Theory of Surface Roughness," *Proc. R. Soc. A. Math. Phys.*, **393**, pp. 133–157.
- [27] Tomanik, E., Chacon, H., and Teixeira, G., 2003, "A Simple Numerical Procedure to Calculate the Input Data of Greenwood–Williamson Model of Asperity Contact for Actual Engineering Surfaces," *Tribol. S.*, **41**, pp. 205–215.
- [28] Yu, N., and Polycarpou, A., 2004, "Extracting Summit Roughness Parameters From Random Gaussian Surfaces Accounting for Asymmetry of the Summit Heights," *ASME J. Tribol.*, **126**(4), pp. 761–766.
- [29] Pawlus, P., 2007, "Digitisation of Surface Topography Measurement Results," *Measurement*, **40**(6), pp. 672–686.
- [30] Suh, A., Polycarpou, A., and Conry, T., 2003, "Detailed Surface Roughness Characterization of Engineering Surfaces Undergoing Tribological Testing Leading to Scuffing," *Wear*, **255**(1–6), pp. 556–568.
- [31] Li, M., Phillips, M. J., and Whitehouse, D. J., 1989, "Extension of Two-Dimensional Sampling Theory," *J. Phys. A. Math. Gen.*, **22**, pp. 5053–5063.
- [32] Poon, C. Y., and Bhushan, B., 1995, "Comparison of Surface Roughness Measurements by Stylus Profiler, AFM and Non-Contact Optical Profiler," *Wear*, **190**(1), pp. 76–88.
- [33] Sayles, R. S., and Thomas, T. R., 1979, "Measurements of the Statistical Properties of Engineering Surfaces," *J. Lubr. Technol.*, **101**, pp. 409–417.
- [34] Wu, J. J., 2000, "Simulation of Rough Surfaces With FFT," *Tribol. Int.*, **33**(1), pp. 47–58.
- [35] ISO 25178 draft standard, "Geometrical Product Specifications—Surface Texture: Areal, Part 2: Terms, Definitions and Surface Texture Parameters.
- [36] Blunt, L., and Jiang, X., 2003, "Numerical Parameters for Characterization of Topography," *Advanced Techniques for Assessment Surface Topography*, L. Blunt and X. Jiang, Eds., Kogan Page Science, London and Sterling, pp. 17–41.
- [37] Kogut, L., and Etsion, I., 2003, "A Finite Element Based Elastic Plastic Model for the Contact of Rough Surfaces," *Tribol. T.*, **46**(3), pp. 383–390.
- [38] Whitehouse, D. J., and Archard, J. F., 1970, "The Properties of Random Surfaces of Significance in Their Contact," *Proc. R. Soc. A. Math. Phys.*, **316**, pp. 97–121.
- [39] Chang, W. R., Etsion, I., and Bogy, D. B., 1987, "An Elastic–Plastic Model for the Contact of Rough Surfaces," *ASME J. Tribol.*, **109**(2), pp. 257–263.
- [40] Patir, N., and Cheng, H. S., 1978, "An Average Flow Model for Determining Effects of Three-Dimensional Roughness on Partial Hydrodynamic Lubrication," *J. Lubr. Technol.*, **100**, pp. 12–17.
- [41] Pawlus, P., and Zelasko, W., 2012, "The Importance of Sampling Interval for Rough Contact Mechanics," *Wear*, **276–277**, pp. 121–129.